Aerodynamic Behavior Prediction of a Twisted Horizontal Axis Wind Turbine Blade

Hassan NAMIR, Mohamed KAMOUNI
Process, Renewable Energy and Environment Laboratory, Sidi Mohamed Ben Abdellah University, Fes, Morocco

Abstract— In order to extract the maximum wind energy, the wind turbine blade geometry should be optimized. In this work, a model was developed to predict the aerodynamic characteristics of a horizontal axis wind turbine (HAWT). The model is based on a two-dimensional steady flow through S-series airfoils developed by the National Renewable Energy Laboratory (NREL). The aerodynamic simulations were performed using a Computational Fluid Dynamics (CFD) method based on the finite-volume approach. The governing equations are the Reynolds-Averaged-Navier-Stokes (RANS) equations completed by a model of turbulence. The model has been validated on the Delft university experimental data and a comparison has been made between three of the most used turbulence models. It has been proven that the k-ω SST model is the best turbulence model in this investigation. Since, lift and drag forces acting on turbine blades are the main parameters in studying wind-turbine performance, an attempt to analyze the trend of these forces at various angles of attacks for three Reynolds numbers cases and for four profiles is presented. The obtained results show that the model used in this work can more accurately calculate these aerodynamic loads compared to other previous predictions. Moreover, the optimum angle of attack has been determined for each profile at different Reynolds numbers.

Index Terms— Airfoil, CFD, Finite volume method, HAWT, RANS, Wind energy.

1 INTRODUCTION

SOLAR radiation heats unevenly and irregularly our planet while creating temperature zones and different atmospheric pressures around the globe. These pressure gradients create air movements which can attack and rotate wind turbines to transform partially the kinetic energy of the wind into usable electrical energy. This category of energy is currently experiencing a significant growth and is widely seen as a serious alternative to fight against the greenhouse effect.

The earlier airfoils used for horizontal-axis wind turbines were originally developed for airplanes. However, the performance of a wind turbine rotor depends on the wind characteristics of the site and the aerodynamic shape of the blades. Many experimental and theoritical research studies have been conducted by many researchers around the world to developp adequate and performant aerodynamic profiles for horizontal-axis wind turbines. To achieve this goal, it is necessary to determine aerodynamic characteristics and the fine structure of the flow through the blades of these wind turbines. Due to difficulties to carry out experiments and the costs associated with the realization of industrial prototypes, numerical modeling and simulation are emerging as key tool to analyze and predict the aerodynamic behavior of this type of machines.

Particularly, in 1995, Yang and al. [1] used a CFD code (computation fluid dynamics) to study and simulate the flow around a bidimensionnal wind turbine blade (NREL phase VI S809 airfoil). They have developped a methodology to analyze the NREL S809 airfoil at various angles of attack (α) from 1 to 45 degrees. Depending on the value of α, their preliminary results showed excellent to fairly good agreement with the experimental data. This work has opened the door to the CFD application in aerodynamics.

Then, in 1997, Somers and al. [2] conducted a theoretical and experimental study on the airfoil S809 in a low turbulence tunnel at Delft University of technology in Netherlands. The objective of this study was to determine the operating conditions for maximum lift, insensitive to roughness, and low drag for a prototype in turbulent flow. Their theoritical results agree with the experimental measurements. Also, Wolfe and Ochs [3] studied the capacity and accuracy of commercial computer code to predict the flow field and the aerodynamic characteristics of the typical wind turbine S809. They made a comparison between their aerodynamic coefficients and the Delft Data ones. They highlighted the need for further investigation to enable the development of digital simulations of flows on wind turbine blades. Their results showed that standard turbulence models used in ancient CFD codes such as (k-ε), are not suitable for excessive angles of attack.

In 2009, Jing and al. [4] have done an experimental and bidimensionnal numerical study of HAWT blade (NREL S809 airfoil), all based on Somers's experiments and Wolfe tips. The optical method of flow visualization PIV "Particle Image Velocimetry" was used in this experiment for different angles of attack under different Reynolds numbers. Relatively good agreement between their experimental and numerical result was achieved.

Recently, in 2015, Xinzi et al. [5] developed an aerodynamic model to obtain the optimal blade chord and twist angle distributions along the blade span for a small wind turbine. This model integrated the profile analysis, Reynolds number effects, tip and hub effects, and drag effects. It was proven that this approach enables seamless link with computational fluid dynamics analysis and CNC manufacturing.

More recently, in Mai 2018, Kaya et al. [6] investigated the aerodynamic performance of Horizontal Axis Wind Turbines with forward and backward swept blades. They developped a model to predict and simulate the changes in power and

thrust coefficients with swept blades of a HAWT. They found that the forward swept blades have the ability of increasing the performance while the backward swept blades tend to decrease the thrust coefficient.

It follows that the prediction of the aerodynamic behavior of wind turbines requires additional efforts to approach the theoretical models to the physical reality. In this context, our contribution tries to meet these attends. It takes part to the development of wind energy through improving efficiency, performance and operating conditions of wind turbines.

2 Computational Model

The aerodynamic modeling of a steady speed flow through two dimensions of some NREL S-series wind-turbine blade profiles is performed using a CFD technique based on the finite-volume approach. The shapes of the different studied profiles were previously used by Tangier and Somers [7] and Somers [8-10]. The airfoil parameters and aerodynamic forces are shown in figure 1 where α is the angle of attack (AOA), C is the profile chord, D is the drag force, L is the lift force, R is the resulting force, and U is the wind speed. The shapes of the selected profiles in this work are shown in figure 2.

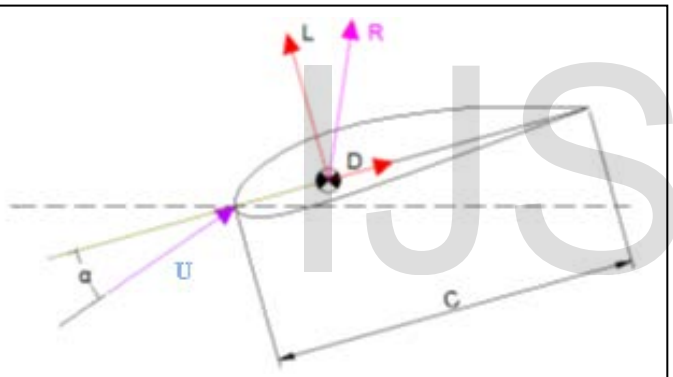

Fig. 1. Geometric model and aerodynamic forces acting on the airfoil

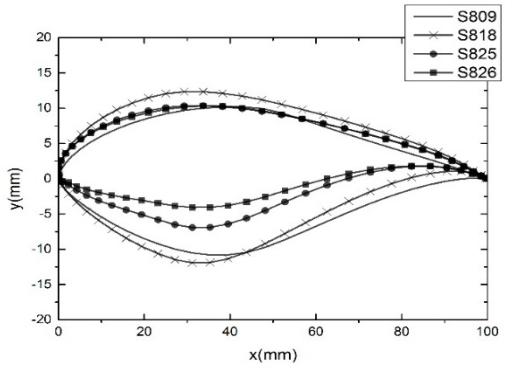

Fig. 2. NREL selected airfoils

The main tasks of the developed model are to analyze the flow structure around the blades of a horizontal axis wind turbine and to predict the lift, drag and pressure coefficients respectively defined as follows:

$$C_l = \frac{L}{1/2\rho U^2 A} \quad (1)$$

$$C_d = \frac{D}{1/2\rho U^2 A} \quad (2)$$

$$C_p = \frac{p - p_\infty}{p_0 - p_\infty} \quad (3)$$

where, A is relevant surface area, ρ is the fluid density , p is the static pressure in the point at which pressure coefficient is being evaluated, p_0 is stagnation pressure in the freestream, and p_∞ is the static pressure in the freestream These coefficients are used to measure the aerodynamic lift and drag forces which are known to vary with the angle of attack and the shape of the airfoil.

In this study, we are interested in the numerical simulation of the air flow around a wind turbine blade exposed to the wind speed for different angles of attack at different S-serie profiles and different Reynolds numbers. The flow is assumed axisymmetric two-dimensional, steady and fully turbulent. The governing equations are the continuity and momentum equations. They can be written in a cartesian coordinate system as:

$$\frac{\partial \rho}{\partial t} + \frac{\partial}{\partial x_i}(\rho u_i) = 0 \quad (4)$$

$$\frac{\partial}{\partial t}(\rho u_i) + \frac{\partial}{\partial x_j}(\rho u_i u_j) = -\frac{\partial p}{\partial x_i} + \frac{\partial}{\partial x_j}\left[\mu\left(\frac{\partial u_i}{\partial x_j} + \frac{\partial u_j}{\partial x_i} - \frac{2}{3}\delta_{ij}\frac{\partial u_l}{\partial x_l}\right)\right] + \frac{\partial}{\partial x_j}(-\rho\overline{u_i' u_j'}) \quad (5)$$

With

$$-\rho\overline{u_i' u_j'} = \mu_t\left(\frac{\partial u_i}{\partial x_j} + \frac{\partial u_j}{\partial x_i}\right) - \frac{2}{3}\left(\rho k + \mu_t \frac{\partial u_k}{\partial x_k}\right)\delta_{ij} \quad (6)$$

The fluctuation terms as Reynolds stresses ($-\rho\overline{u_i' u_j'}$) are represented and modeled by a turbulence model in order to complete and close this system of equations [11-13]. Different turbulence models were used and compared [Spalart-Allmaras, k-ε and k-ω SST] to find the appropriate model for this kind of aerodynamic flow.

3 Mesh Topology And Operating Conditions

The shape and discretization of the computational domain have been optimized to correctly describe the physical events and to get a suitable calculation time and precision. The mesh used is is shown in figure 3. It is a C-type grid topology, including non-uniform quadrilateral cells, which is becoming

finer and denser near the airfoil surface.

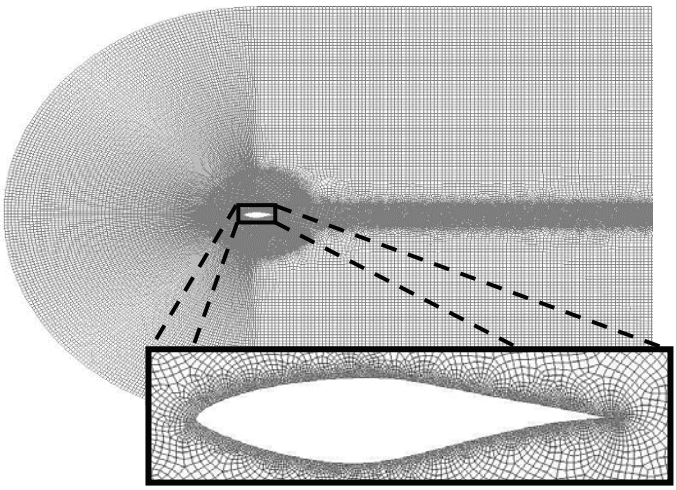

Fig. 3. The used optimised mesh

The material used in the computational domain is ambient air with the operating conditions summurized in table 1.

4 Results And Discussion

The purpose of this simulation is to determine the

TABLE 1
TURBINE OPERATING CONDITIONS

Quantity	Units
Wind speed	30 m/s
Air density	1.225 kg/m^3
Atmospheric pressure	101325 Pa

responsible flow field forces acting on the wind turbine blade and to compare them for some famous airfoils. Figures 4 and 5 show the variation of the experimental and theoretical lift and drag coefficients of S809 airfoil, all depending on the angle of attack for three turbulence models (Spalart Allmaras, K-ε and k-ω SST) at a Reynolds number [Re=2.106]. Firstly, these figures show that all coefficients values obtained with the k-ω SST model are the closest to those obtained by experiment. Secondly, these figures show that our model describes better these aerodynamic features compared to previous Wolfe's works, especially for relative big angles of attack (α >7°).

Moreover, these curves show that the angle of attack must be between 10° and 15° to obtain a maximum lift coefficient C_l. However, in this area the drag coefficient C_d becomes also larger, which makes the optimum angle of attack situated between 7° and 10°.

Since, it is interesting to minimize the drag coefficient and in the same time to maximize the lift one, the C_l/C_d ratio is used to compare the lift effect of C_l to the drag effect of C_d.

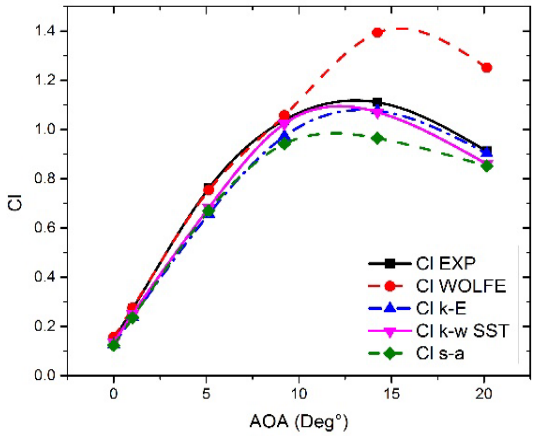

Fig. 4. Lift coefficient C_l in terms of the angle of attack for several turbulence models compared to experiment (S809 airfoil).

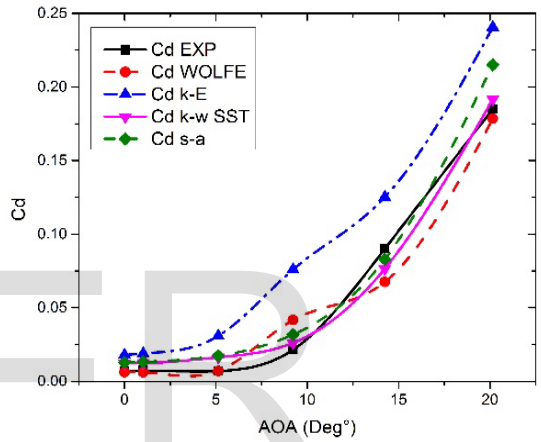

Fig. 5. Drag coefficient C_d in terms of the angle of attack for several turbulence models compared to experiment (S809 airfoil).

Figures 6, 7 and 8 present this ratio in terms of the angle of attack for the already mentioned airfoils at Reynolds number equals to 1.10^6, 2.10^6 and 3.10^6, respectively. Firstly, these figures show that the C_l/C_d ratio starts to increase gradually with increasing the angle of attack. Then, this ratio tumbles down clearly for the all profiles when α exceeds 9° except for the S826 airfoil for which the tumble starts from α equals 7°.

Moreover, one can easily see that the S826 profile has a C_l/C_d ratio much better than other profiles when (α < 10°), at all wind speed cases. Although, for higher angles of attack (α > 10°), both of S818 and S825 profiles become the best. In addition, the figures show that the profile S809 seems to have the lowest ratio. However, for medium angles of attack (9° ≤ α ≤ 18°), the best solution is distributed between the S825 and S818 profiles. For (9° ≤ α ≤ 13°), the profile S825 becomes the best in all Reynolds number cases. For (13° < α ≤ 18°), the S825 profile remains the best at low speeds (Re < 2.10^6) but the S818 profile becomes the best at high speeds (Re ≥ 2.10^6).

Furthermore, it can be noted that these obtained results make here the profile S809 useless in all angle of attack zones.

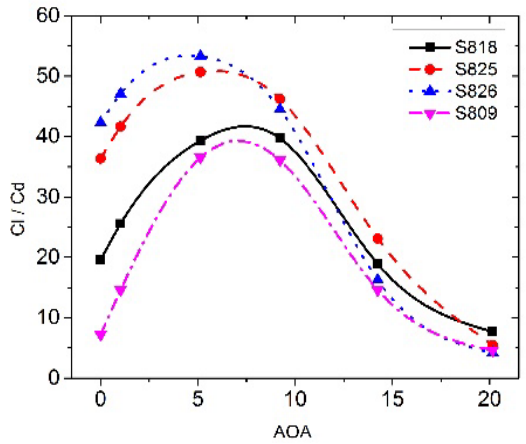

Fig. 6. C_l/C_d ratio versus the angle of attack for the four airfoils at Re=1.10^6.

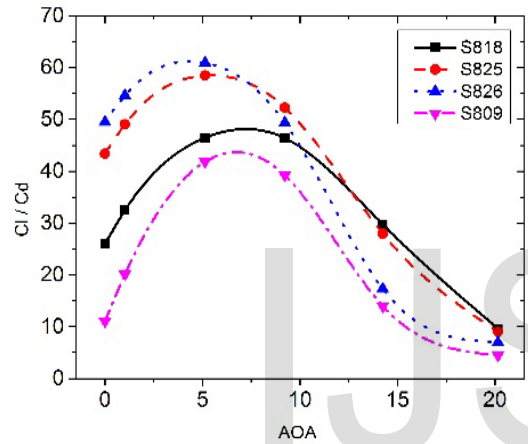

Fig. 7. C_l/C_d ratio versus the angle of attack for the four airfoils at Re=2.10^6.

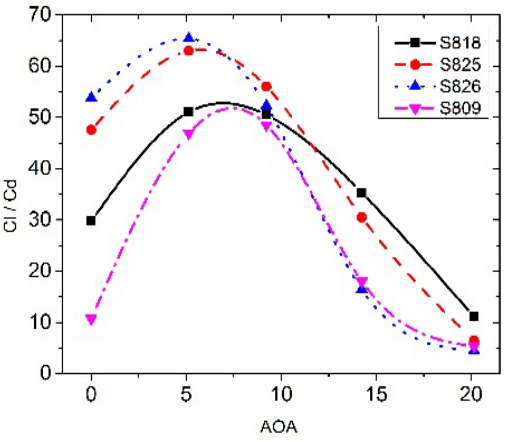

Fig. 8. C_l/C_d ratio versus the angle of attack for the four airfoils at Re=3.10^6.

Figures 9, 10 and 11 represent the pressure coefficient distribution along the chord length for the three optimum airfoils at α=5°, α=12° and α=14°, respectively. The bottom line of each closed curve of these figures represents the pressure coefficient distribution in the airfoil's upper surface [Extrados], which means that the extrados represents the low-pressure area. The top line of each closed curve represents the pressure coefficient distribution in the airfoil's bottom surface [intrados], namely the lower surface is the high-pressure zone. Additionally, these figures also show that while increasing the angle of attack, a large pressure difference between extrados and intrados is created to generate high aerodynamic forces. Figure 9 shows that the large pressure difference occurs for the S826 profile at α=5° while figure 10 shows that the S825 profile generates the largest pressure difference at α=12°. Figure 11 shows that the S818 profile provides the large pressure difference at α=14°. Otherwise, it can be noted that these results confirm the already obtained results concerning lift and drag coefficients.

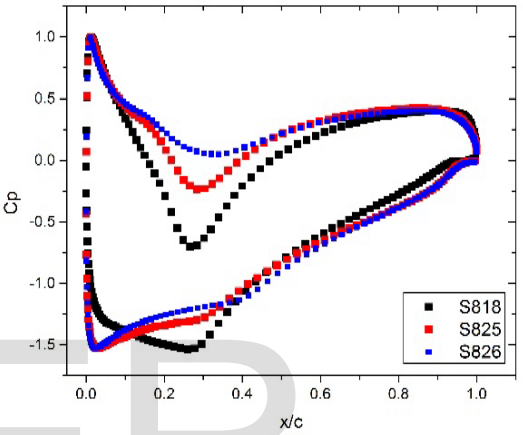

Fig. 9. Pressure coefficient C_p along the selected airfoils for α = 5°.

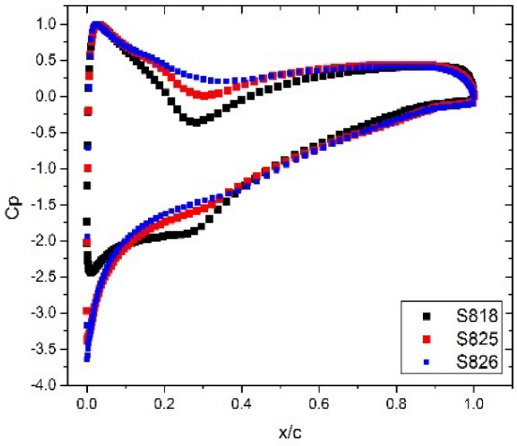

Fig. 10. Pressure coefficient C_p along the selected airfoils for α = 12°.

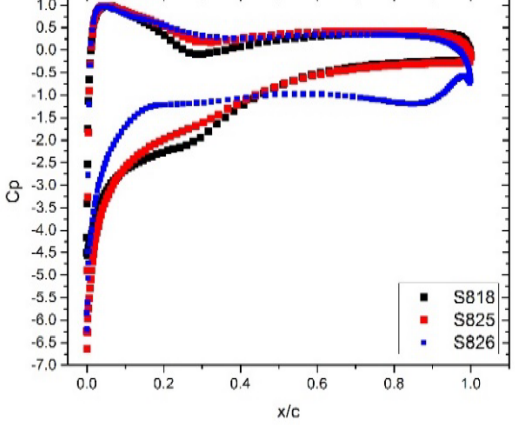

Fig. 11. Pressure coefficient C_p along the selected airfoils for α = 14°.

Figures 12, 13 and 14 show the velocity contours around the selected airfoil S826 at different angles of attack 5°, 12°and 25°, respectively. Once again, these figures show that due to the pressure distribution at lower and upper airfoil surfaces, the velocity values in the intrados are less important than those in the extrados.

The velocity contours in figure 12 show that for low angles of attack (α = 5°), the flow is attached with no separation point. However, when the angle of attack becomes enough important (α = 12°) as in figure 13, the flow separation bigins to occur while the attached flow is still dominant. Even more, velocity contours in figure 14 show that for high angles of attack (α = 25°), an important stall effect arises and the separated flow is so dominant that additional increases in angle of attack produce less lift and more drag.

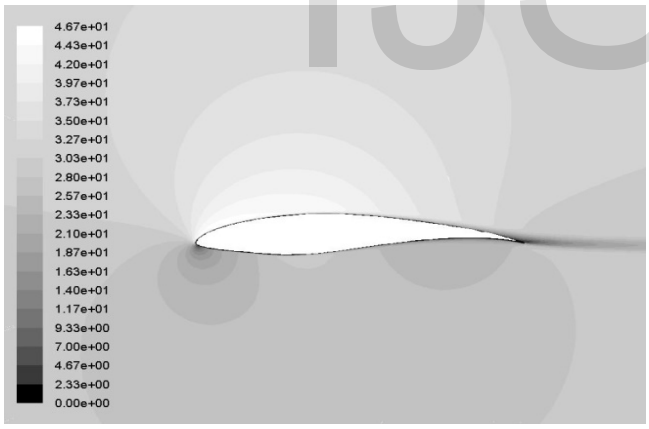

Fig. 12. Velocity contours of S826 airfoil for α = 5°.

Fig. 13. Velocity contours of S826 airfoil for α = 12°.

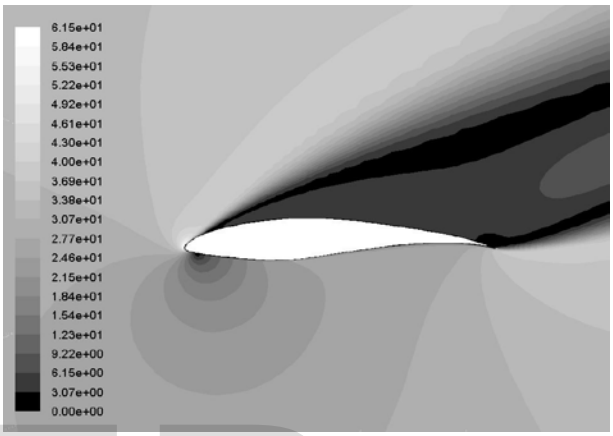

Fig. 14. Velocity contours of S826 airfoil for α = 25°.

In summary, we can say that the primary fixed objectives of this study have been achieved. According to the obtained results in this work, a twisted blade may be made using several profiles combined as follows: the S818 is the favorite profile for high angles of attacks, so it should be near the cylinder root to get the biggest twist on this blade. Then, this profile will be followed by the S825 one which is relatively the best profile for average angles of attack (9° < α < 14°). Then again, a transition to the S826 profile should be taken into account for lower angles of attack. The three-dimensional geometry of the optimal twisted blade combining the three studied profiles is shown in figure 15.

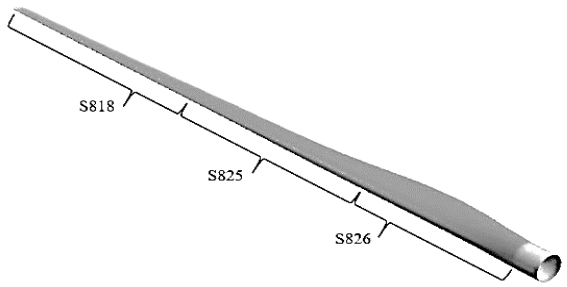

Fig. 15. Three-dimensional twisted blade combining S818, S825 and S826 airfoils.

Moreover, figures 16 and 17 describe qualitatively primary results relating to airflow through this multi-profile blade. Figure 16 shows the velocity vectors along the blade. We can easily see that the minimum velocity of the flow is located near the root of the blade and this velocity increases with increasing the turbine radius to get its maximum value at the tip of the blade.

Figure 17 shows the fluid pressure distribution around the blade in three radial positions located at the root, the middle and the tip of the blade. We can see that the pressure drops from the root to the tip along the blade. Additionally, these three pressure contours show that the pressure values in the extrados are less important than those in the intrados.

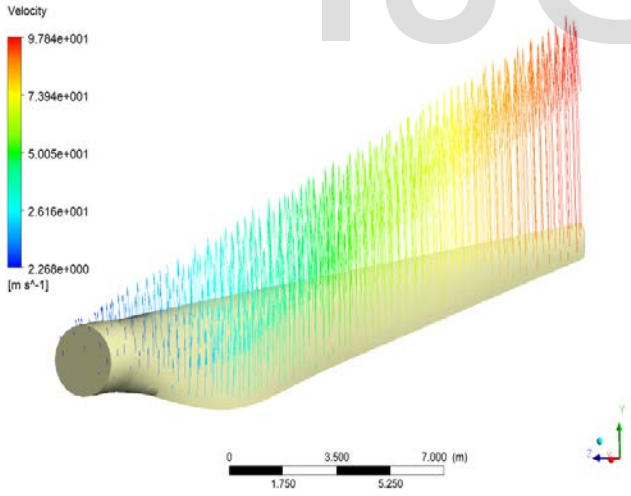

Fig. 16. Velocity vectors along the blade.

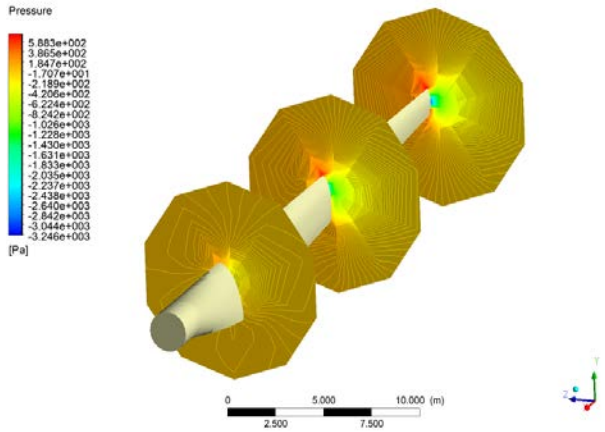

Fig. 17. Three local fluid pressure contours around the blade.

5 Conclusion

In this paper, a model has been developed to predict aerodynamic coefficients and optimal operating conditions of a horizontal axis wind turbine crossed by a two-dimensional air flow. In general, the model predictions are in good agreement with experimental data of Smers (Delft data). It is shown that the blade profile shape has a fundamental effect on the aerodynamic performance of this kind of wind turbines.

The obtained results show that the optimum angle of attack corresponding to a significant lift and low drag is mostly between 5° and 9° and that the stall effect becomes important when this angle exceeds 14°. In addition, four famous NREL airfoils [S809, S818, S825 and S826] are selected to compare the angle of attack effect at three Reynolds numbers on the aerodynamic characteristics of this wind turbine. We have found that in all Reynolds number cases, the S826 profile is the best for small angles of attack ($a < 9°$) while the S818 profile remains the good solution for high angles of attack ($a > 18°$). However, for medium angles of attack ($9° \leq a \leq 18°$), the best solution is distributed between the S825 and S818 profiles. For ($9° \leq \alpha \leq 13°$), the profile S825 becomes the best in all Reynolds number cases. For ($13° < \alpha \leq 18°$), the S825 profile remains the best at low speeds ($Re < 2.10^6$) but the S818 profile becomes the best at high speeds ($Re \geq 2.10^6$). We also note that these obtained results make here the profile S809 useless in all angle of attack zones.

Furthermore, while considering these results, an optimal blade geometry solution could be obtained by adequatly combining the three airfoils [S818, S825 and S826] in a unique twisted blade.

References

[1] Yang S. L., Chang Y. L., Arici O., "Navier-Stokes Computations of the NREL Airfoil Using a $\kappa - \omega$ Turbulent Model at High Angles of Attack", ASME, Vol 117, pp.304-310, 1995

[2] Somers D.M., "Design and Experimental Results for the S809 Airfoil", NREL Report, DE-AC36-83CHlO093, January 1997.

[3] Wolfe W.P. Ochs, S.S., "CFD calculations of S809 aerodynamic characteristics", Sandia Report AIAA-97-0973, United States of America, 1997.

[4] Jing M., Guo R., Jinglei X., Zhang K. (2009), "Piv experimental and numerical study of a 2-D airfoil for wind turbines", 978-1-4244-4702-2/09/ ©IEEE, 2009.

[5] Xinzi Tang, Xuanqing Huang, Ruitao Peng and Xiongwe Liu," A Direct Approach of Design Optimization for Small Horizontal Axis Wind Turbine Blades", Procedia CIRP 36, pp, 12–16, 2015.
[6] Kaya M.N, Kose F, Ingham D, Ma L and Pourkashanian M, " Aerodynamic performance of a horizontal axis Wind Turbine with forward and backward swept Blades", Journal of Wind Engineering & Industrial Aerodynamics, Vol 176, pp.166–173, 2018.
[7] Tangier J.L., Somers D.M., "NREL Airfoils Families for HAWTs", NRELfTP-442-7109, January 1995.
[8] Somers D.M., "The S816, S817, and S818 Airfoils", NREL/SR-500-36333, January 2004.
[9] Somers D.M., "Design and Experimental Results for the S825 Airfoil", NREL/SR-500-36346, January 2005.
[10] Somers D.M., "The S825 and S826 Airfoils", NREL/SR-500-36344, January 2005.
[11] Spalart P.R., Allmaras S.R., "A One-Equation Turbulence Model for Aerodynamic Flows", AIAA Paper, 92-0439, 1992.
[12] Wilcox D.C., "Re-assessment of the scale-determining equation for advanced turbulence models", AIAA Journal, Vol. 26, pp. 1414-1421, 1988.
[13] Menter F.R., "Two-Equation Eddy-Viscosity Turbulence Models for Engineering Applications", AIAA Journal, Vol. 32, pp. 1598-1605, 1994.